Demonstration of an air-slot mode-gap confined photonic crystal slab nanocavity with ultrasmall mode volumes

Jie Gao,[1,a)] James F. McMillan,[1] Ming-Chung Wu,[1] Jiangjun Zheng,[1] Solomon Assefa,[2] and Chee Wei Wong[1,a)]
[1]*Optical Nanostructures Laboratory, Columbia University, New York, New York 10027, USA*
[2]*IBM TJ Watson Research Center, Yorktown Heights, New York 10598, USA*

(Received 8 September 2009; accepted 23 December 2009; published online 5 February 2010)

We demonstrate experimentally an air-slot mode-gap photonic crystal cavity with quality factor of 10^4 and modal volume of 0.02 cubic wavelengths, based on the design of an air-slot in a width-modulated line-defect in a photonic crystal slab. The origin of the high Q air-slot cavity mode is the mode-gap effect from the slotted PhCWG mode with negative dispersion. The high Q cavities with ultrasmall mode volume are important for applications such as cavity quantum electrodynamics, nonlinear optics, and optical sensing. © *2010 American Institute of Physics*. [doi:10.1063/1.3298642]

Photon confinement and processes in optical cavities are critical for a vast span of fundamental studies and applications. Many optical cavities with high quality factor (Q) and small mode volume (V) have been developed and fabricated, including Fabry–Perot cavities,[1] microspheres,[2] silicon and silica whispering gallery type resonators,[3,4] and photonic crystal nanocavities.[5,6] In particular, the two-dimensional (2D) photonic crystal cavity with a single emitter possesses remarkable possibilities toward efficient single photon sources or strong coupling regime for quantum communications and computing. Silicon photonic crystal cavities have achieved remarkable Q up to $\sim 10^6$ experimentally but with mode volume traditionally limited to sizes that are on the order of the wavelength of light. From the definition of the normalized dimensionless effective mode volume

$$V_{\text{eff}} = \frac{\int \varepsilon(\vec{r})|\vec{E}(\vec{r})|^2 d^3r}{\varepsilon(\vec{r}_{\max})\max[|\vec{E}(\vec{r})|^2]}\left(\frac{2n(\vec{r}_{\max})}{\lambda}\right)^3$$

(where $\vec{r}_{\max}$ is the location of the maximum squared electric field), we know that mode volume can be reduced by increasing the mode maximum electric filed and localizing the mode maximum in the low index region. Reducing V_{eff} in cavities enables one to control the degree of light-matter interaction for processes such as nonlinear optics[7] and cavity quantum electrodynamics (QED).[8] The Purcell factor for an emitter in a resonant cavity is inversely proportional to V_{eff},[9] and the Rabi frequency is inversely proportional to the square root of V_{eff}.[10] Toward this objective, Robinson *et al.*[11] have proposed one-dimensional (1D) microcavities with ultrasmall mode volume by using dielectric discontinuities with subwavelength dimensions as a means of local field enhancement. Under the same idea, our previous work designed and measured an air-slot L3 cavity with ultrasmall mode volume through tapered fiber coupling.[12] However quality factors of air-slot L3 or 1D photonic crystal cavities are typically not very high because the structures suffer large vertical radiation loss at the abrupt termination of the air-slot. In this letter, we examine mode-gap confined nanocavities in a 2D photonic crystal slab with a nonterminated air-slot, which have both high Q and ultrasmall mode volume for the study of light matter interaction.

We experimentally study air-slot mode-gap photonic crystal cavities based on the original proposal in Ref. 13. A nonterminated air-slot is added to width-modulated line-defect photonic crystal cavities (shifting air holes away from waveguide[14]) to create ultrasmall mode volume cavities. However, other work on high Q heterostructure air-slot cavities[15] emphasize the positive dispersion of slotted PhCWG mode and form the cavities by locally compressing the lattice to pull the eigenstate up in the band gap, opposite to conventional mode-gap cavities.[14,16] To better understand the modes, we first investigate the modes and dispersion in slotted PhCWG. We perform three-dimensional band structure calculation for slotted W1 waveguide in Fig. 1(a). Three modes are shown in Figs. 1(b-I, -II, and -III). Compared with the field distribution of standard W1 PhCWG, Mode I and II can be, respectively, traced back to W1 waveguide fundamental even mode and high order odd mode inside the band gap.[17,18] The electric field of mode I inside the air slot region is the *Ey* component and the existence of air slot enhances this component because the electric displacement in *y* direction needs to be continuous across the slot boundary. However, the electric filed of mode II inside the air slot region is the *Ex* component and is not affected since its polarization is parallel to the slot. This also explains why mode I appears closer to the air band, and even has higher frequency than

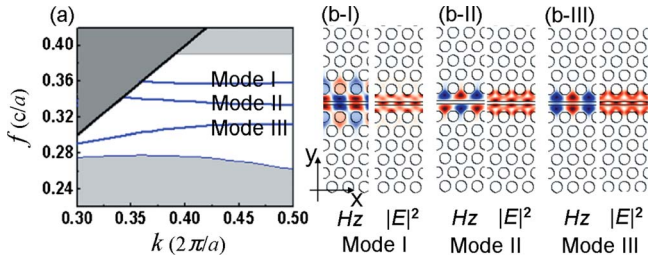

FIG. 1. (Color online) (a) Band structure of slotted W1 PhCWG with a=490 nm, r=0.34a, t=0.449a, n_{si}=3.48, and slot width s=80 nm. (b-I,II,III) Field distributions (Left: H_Z; Right: $|E|^2$) of the three modes inside TE band gap.

a)Authors to whom correspondence should be addressed. Electronic addresses: jg2499@columbia.edu and cww2104@columbia.edu.

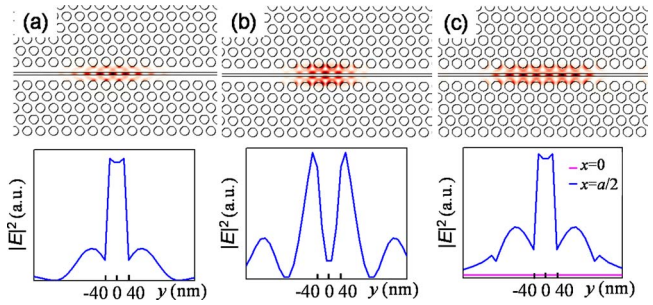

FIG. 2. (Color online) [(a)–(c)] 2D FDTD simulation of $|E|^2$ spatial distribution and the $|E|^2$ value across the air slot for cavity modes created from photonic waveguide mode I, II, and III, respectively.

mode II. Note that we have mode III in the band gap, which shows a positive slope in the first Brillouin zone. While the mode is similar to the mode discussed in Ref. 19, the origin of this mode is not well explained earlier. By comparing the *Hz* field of mode III with the index-guided modes in W1 waveguide, we note mode III actually originates from the second index-guided mode shown in Ref. 17 below the projected bulk modes. This mode has *Ey* component in the slot, and so the frequency is pulled up to be within the photonic band gap.

When we generate cavities by locally shifting the air holes away from the center of waveguide, a mode-gap region is formed and cavity modes are created just below the slotted PhCWG transmission band. There are three possible modes (Fig. 2). Confirmed from the mode frequency and symmetry, mode in Fig. 2(a) is due to the mode gap of slotted waveguide mode I in Fig. 1 (b-I) and is expected to have both high Q and ultrasmall V. This is also the only accessible high Q mode in the experiment through even mode excitation (from strip waveguide). The normal component of the electric displacement is continuous across the boundary of the air-slot walls, thus $\varepsilon_0 E_{air} = \varepsilon_{si} E_{si}$. The mode maximum squared electric field is in the air-slot center region [Fig. 2(a)]. Compared with mode-gap confined cavities without slot, the slot cavity $\max|\vec{E}(\vec{r})|^2$ is increased by $\varepsilon_{si}/\varepsilon_0 = n_{si}^2$ with an infinitesimal slot. Together with $n(\vec{r}_{max})=1$, the dimensionless effective mode volume shows a total decrease of $n_{si}^5 \sim 510$ times stronger localization. Figure 2(b) represents the mode with the same odd symmetry as mode II in slotted waveguide, and Fig. 2(c) represents the low Q mode which couples to PhCWG mode III without mode-gap confinement.

An example scanning electron micrograph (SEM) of the electron-beam nanofabricated cavity is illustrated in Fig. 3(a), with 220 nm thick Si and suspended with a sacrificial wet-etch.[20] Three-dimensional (3D) finite-difference time-domain (FDTD) simulations evaluate the fabricated cavity

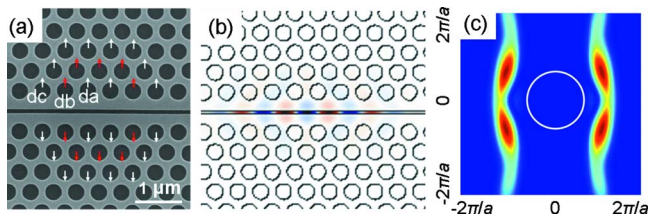

FIG. 3. (Color online) (a) SEM of the air-slot mode-gap confined cavity. (b) and (c) 3D FDTD simulation and Fourier transform of the electric field for cavity mode due to mode-gap effect of waveguide mode I.

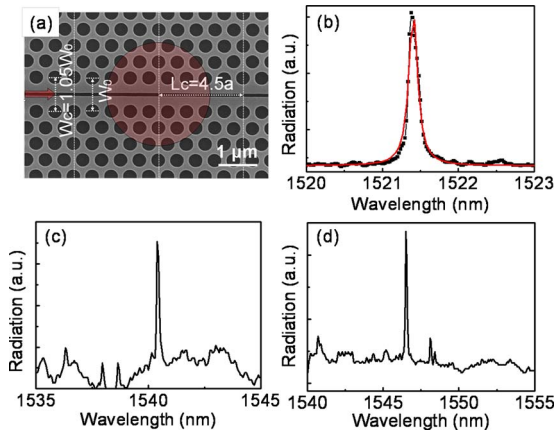

FIG. 4. (Color online) (a) SEM of the air-slot mode-gap confined cavity with in-line coupling waveguide. The base width of a line defect $W_0=\sqrt{3}a$ and the width of input/output waveguides is $Wc=1.05\times\sqrt{3}a$. The distance between the cavity and coupling waveguide is $L_C=4.5a$. Large circle (red) indicates the region from which the radiation signals are collected. [(b)–(d)] Radiation spectra of three devices: (b) $W_0=\sqrt{3}a$, $s=80$ nm, and $r=0.306$; (c) $W_0=\sqrt{3}a$, $s=80$ nm, and $r=0.285$; (d) $W_0=1.2\times\sqrt{3}a$, $s=120$ nm, and $r=0.285$.

mode properties with $a=490$ nm, $r=0.34a$, $t=0.449a$, $n_{si}=3.48$, $da=0.0286a$, $db=0.019a$, and $dc=0.0095a$. For slot width $s=80$ nm (grid spacing at 28 nm), the cavity supports a high Q localized even mode [see Fig. 3(b)] with Q factor of 1.6×10^5 and mode volume V of $0.02(\lambda/n_{air})^3$. The Q/V ratio of $8\times10^6(\lambda/n_{air})^{-3}$ is much higher than previous reported ultrasmall mode volume cavity designs.[11,12,21] Furthermore, the electric field 2D Fourier transform [Fig. 3(c)] shows small leaky components inside the light cone supporting the high Q character. An in-line PhCWG coupling configuration was utilized to the cavity, with cavity-waveguide distance $L_C=4.5a$ for tunneling [SEM in Fig. 4(a)]. The base widths of a line defect for a cavity is $\sqrt{3}a$ and the input/output waveguides are $1.05\times\sqrt{3}a$. Polarization controllers, lensed fibers, and tunable lasers are used for the transverse-electric (TE) polarization launched. Vertical cavity radiation is collected [red region in Fig. 4(a)] by a 40× objective lens with lock-in amplification to analyze the cavity resonances and Q from the radiation linewidth. Figures 4(b)–4(d) illustrate the measured cavity linewidth for different slot widths (80 and 120 nm) and hole radius ($r=0.306a$ and $0.285a$).

For the 80 nm slot width devices, Fig. 4(b) shows a 0.13 nm linewidth from Lorentzian fit for a Q of ~12 000. The measurements are one order of magnitude smaller than the 3D FDTD simulation due to variations of the slot width and roughness of slot edge during fabrication, which degrade the cavity Q. For cavity with smaller hole radius, the band gap and cavity resonance shifts toward longer wavelength [Figs. 4(b) and 4(c)]. When the slot width increases to 120 nm, cavity mode shifts close to the air band and becomes very lossy. It is expected that cavity resonance moves to shorter wavelength and Q factor drops significantly. However, we increase the width of the base waveguide in this case to be $1.2\times\sqrt{3}a$. This maintains the cavity mode in the middle of the band gap, resulting with measured Q of ~15,000 [Fig. 4(d)]. More air-slot cavities with various parameters are examined and quality factors are observed within the range of 12 000–25 000.

This experimental demonstration of air-slot mode-gap cavity with both high Q and ultrasmall mode volume provides us a platform to advance cavity QED based on colloidal nanocrystals and silicon nanocavities. Compared to InAs quantum dots, colloidal nanocrystals can be spun on silicon nanocavities as a post-CMOS hybrid integration process. Moreover lead salt nanocrystals can operate at the longer near- to mid-infrared wavelengths. Purcell factor of up to 300 is possible for air-slot mode-gap confined cavity (with $Q_c \sim 1.6 \times 10^5$, $V_{\text{eff}} \sim 0.02$) with PbS nanocrystals on the surface of the slot edge (assuming the exciton dipole decay rate is much smaller compared to g, κ), while previous work[8,22] only show the possibility of 7 to 30 for single-defect photonic crystal nanocavities (such as L3 cavity with $Q \sim 2.6 \times 10^5$, $V_{\text{eff}} \sim 0.7$).[23] Here we estimate the emitter-cavity field coupling strength $g = \mu/\hbar\sqrt{\hbar\omega/2\varepsilon V_{\text{eff}}} \sim 32$ GHZ, and strong coupling is achievable if the air-slot mode-gap photonic crystal cavities possess $Q \sim 3 \times 10^4$. These illustrate the strong potential of the slot cavity colloidal nanocrystal system to achieve high efficiency single photon source on-demand and even strong exciton-photon coupling in the fiber network communication frequencies.

In summary, 2D mode-gap air-slot photonic crystal cavities from the negative dispersion waveguide mode have been fabricated and experimentally characterized with Q up to $\sim 10^4$ and mode volume as small as $0.02(\lambda/n_{\text{air}})^3$. Furthermore we discuss the modes existing in the slotted PhCWGs and explain in detail the origins of the air-slot mode-gap confined cavities modes. The air-slot cavity reported here can strongly enhance light-matter interactions, such as the increased Purcell factor and Rabi frequency in fundamental cavity QED studies.

The authors thank Xiaodong Yang, Chad A Husko, and Ying Li for helpful discussions. We acknowledge funding support from the National Science Foundation CAREER Award No. NSF ECCS 0747787), DARPA MTO, and the New York State Office of Science, Technology and Academic Research.

[1] K. J. Vahala, Nature (London) **424**, 839 (2003).
[2] I. S. Grudinin, A. B. Matsko, and L. Maleki, Opt. Express **15**, 3390 (2007).
[3] M. Soltani, S. Yegnanarayanan, and A. Adibi, Opt. Express **15**, 4694 (2007); S. Xiao, M. H. Khan, H. Shen, and M. Qi, *ibid.* **15**, 14467 (2007); A. Nitkowski, L. Chen, and M. Lipson, *ibid.* **16**, 11930 (2008); J. Gao, P. Heider, C. J. Chen, X. Yang, C. A. Husko, and C. W. Wong, Appl. Phys. Lett. **91**, 181101 (2007).
[4] D. K. Armani, T. J. Kippenberg, S. M. Spillane, and K. J. Vahala, Nature (London) **421**, 925 (2003).
[5] S. Noda, M. Fujita, and T. Asano, Nat. Photonics **1**, 449 (2007).
[6] T. Tanabe, M. Notomi, E. Kuramochi, A. Shinya, and H. Taniyama, Nat. Photonics **1**, 49 (2007).
[7] X. Yang and C. W. Wong, Opt. Express **15**, 4763 (2007).
[8] R. Bose, X. Yang, R. Chatterjee, J. Gao, and C. W. Wong, Appl. Phys. Lett. **90**, 111117 (2007); R. Bose, J. Gao, J. F. McMillan, F. W. Sun, X. Yang, C. J. Chen, and C. W. Wong, Opt. Express **17**, 22474 (2009).
[9] K. Srinivasan and O. Painter, Phys. Rev. A **75**, 023814 (2007).
[10] D. Englund, D. Fattal, E. Waks, G. Solomon, B. Zhang, T. Nakaoka, Y. Arakawa, Y. Yamamoto, and J. Vuckovic, Phys. Rev. Lett. **95**, 013904 (2005).
[11] J. T. Robinson, C. Manolatou, L. Chen, and M. Lipson, Phys. Rev. Lett. **95**, 143901 (2005).
[12] J. Gao, X. D. Yang, W. Green, Y. Vlasov, S. Assefa, and C. W. Wong, Proceedings of Conference of Lasers and Electro-Optics/Quantum Electronics and Laser Sciences, Baltimore, Maryland, 2009 (unpublished).
[13] T. Yamamoto, M. Notomi, H. Taniyama, E. Kuramochi, Y. Yoshikawa, Y. Torii, and T. Kuga, Opt. Express **16**, 13809 (2008).
[14] E. Kuramochi, M. Notomi, S. Mitsugi, A. Shinya, and T. Tanabe, Appl. Phys. Lett. **88**, 041112 (2006).
[15] A. Di Falco, L. O'Faolain, and T. F. Krauss, Appl. Phys. Lett. **94**, 063503 (2009).
[16] B. Song, S. Noda, T. Asano, and Y. Akahane, Nature Mater. **4**, 207 (2005).
[17] C. Jamois, R. B. Wehrspohn, L. C. Andreani, C. Hermann, O. Hess, and U. Gösele, Photonics Nanostruct. Fundam. Appl. **1**, 1 (2003).
[18] J. D. Joannopoulos, S. G. Johnson, J. N. Winn, and R. D. Meade, *Photonic Crystals: Molding the Flow of Light*, 2nd ed. (Princeton University Press, Princeton, 2008).
[19] A. Di Falco, L. O'Faolain, and T. F. Krauss, Appl. Phys. Lett. **92**, 083501 (2008); J. Wu, C. Peng, Y.-P. Li, and Z.-Y. Wang, Chin. Phys. Lett. **26**, 014209 (2009).
[20] S. Assefa, S. J. McNab, and Y. A. Vlasov, Opt. Lett. **31**, 745 (2006).
[21] Z. Zhang and M. Qiu, Opt. Express **12**, 3988 (2004).
[22] I. Fushman, D. Englund, and J. Vuckovic, Appl. Phys. Lett. **87**, 241102 (2005).
[23] Y. Akahane, T. Asano, B. Song, and S. Noda, Opt. Express **13**, 1202 (2005).